APPENDIX D — NUMERICAL MODELING

This appendix reports results of the numerical modeling undertaken in conjunction with the centrifuge modeling and field-scale testing of the SMSE system, as reported in appendices B and C, respectively. A numerical modeling approach was adopted to establish a qualitative means of assessing load-deformation behavior up to failure, given the relatively low level of deformation observed in the field-scale test.

Numerical modeling was limited to the unconnected portion of the field-scale test wall for assessment purposes. The two-dimensional finite element code *PLAXIS* was used to perform the numerical analyses.[64]

D.1 PRELIMINARY WORK

Use of numerical techniques based on the finite element method to assess geosynthetic reinforced wall performance has been limited given the prevalence of design methods based on limiting equilibrium concepts. Given that the accuracy of limiting equilibrium design methods in predicting loads in geosynthetic reinforcement is considered to be poor, their use as a comparative basis for finite element predictions was not pursued.[65] A review of literature regarding previous finite element studies of geosynthetic reinforced walls, suggests a general lack of consensus as to what modeling parameters or approaches are appropriate. In view of these analysis issues and the unique nature of the SMSE wall system tested, preliminary work was undertaken to first confirm the ability of the *PLAXIS* software to simulate geogrid and soil interaction. This was then followed by various trial analysis runs modeling the field-scale test to assess the modeled behavior and to establish the most effective modeling strategy for analyzing the field-scale test.

D.1.1 Geogrid Pullout Simulation

Simulation of a hypothetical pullout test was first undertaken using the model llustrated in figure 82. Pullout was simulated by applying displacement to the end of a central uniaxial “geogrid” element with accompanying “interface” elements placed within a confined, rectangular soil mass. Soil was modeled using an elastic perfectly plastic constitutive formulation where a linearly elastic, isotropic material was assumed for elastic response, and plastic behavior modeled using Mohr-Coulomb shear strength (i.e., $c' - \phi'$ characterization) and zero tensile strength as failure criteria (referred to as the “Mohr-Coulomb” model in *PLAXIS*). Interaction performance was assessed by inspecting the axial force mobilized at the pulled end of the geogrid and distribution of axial displacement along the geogrid element with increasing displacement. Discretization effects were also investigated by using both medium and very fine mesh coarseness for the soil zone.

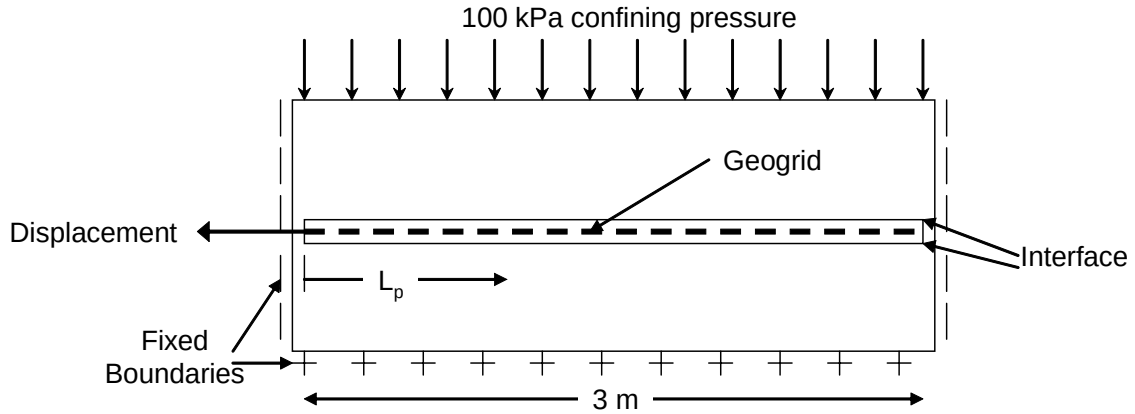

Figure 82. Diagram. Geogrid pullout simulation model set-up.

Results of the analysis are tabulated in table 13 and plots indicating increasing development lengths with increasing load levels are presented in appendix E. Also included in appendix E are plots showing the modeled soil behavior as characterized by the development of plastic points defining either shear or tensile failure. These latter plots indicated a progressive development of soil failure consistent with the variation of development length with increasing load levels in the geogrid.

Table 13. Results of geogrid pullout simulation.

Model	Geogrid Displacement (m)	Development Length[1] (m)	Max. Axial Force (kN/m)
Very fine mesh	0.005	0.20	27
	0.010	0.34	40
	0.015	0.45	50
	0.02	0.55	58
	0.05	0.96	95
	0.10	1.40	137
	0.20	2.01	197
Medium mesh	0.005	0.22	26
	0.010	0.36	40
	0.015	0.47	50
	0.02	0.55	58
	0.05	0.97	94
	0.10	1.40	137
	0.20	2.00	197

[1] Development length is defined as the length at which horizontal movement of the geogrid is approximately 1 mm.

Overall, the pullout simulation results agreed qualitatively with observed pullout behavior, indicating appropriate performance of geogrid-soil interaction by *PLAXIS* in a mechanistic sense. The minor differences in tabulated values apparent for the different mesh configurations also provided confirmation of appropriate discretization for modeling of the field-scale test.

D.1.2 Modeling Issues

Preliminary trials undertaken to assess model performance identified several modeling issues associated with the SMSE wall system. These involved the provision of appropriate stress-strain (stiffness) behavior for the soil, modeling of the welded wire facing units used to support the wall face for each lift of wall construction, and accounting for compaction effects.

Soil Stiffness

In contrast to the pullout simulation exercise, initial attempts at modeling soil behavior using the Mohr-Coulomb model in *PLAXI*S proved ineffective for the SMSE wall system. Repeated failure of the modeled MSE wall was exhibited due to either premature soil failure coupled with insufficient mobilization of geogrid reinforcement, or excessive deformation, depending on the stiffness assigned to the soil. Essentially, the bilinear characterization of stress-strain behavior (i.e., constant stiffness and strength idealization) was considered inadequate for modeling the apparent geogrid-soil interaction developed during construction. Subsequent implementation of a hyperbolic stress-strain characterization for the soil, using the "Hardening-Soil" model in *PLAXIS*, succeeded in providing the necessary improvement for this aspect of the analysis.

MSE Wall Facing

Modeling of the welded wire facing units posed additional challenges. Their self-stabilizing nature brought about by the diagonal wire component (i.e., strut) affixed at nominal 600 mm center-to-center spacing necessitated the inclusion of equivalent "anchor" elements at the top of each facing unit for modeling purposes. This anchor element provided a restraining stiffness afforded by the diagonal component in both tension and compression (the latter considered possible due to soil confinement). While the constructed configuration provided for possible independent movement of each facing unit, the continuum formulation inherent in *PLAXIS* prevented direct modeling of this constructed feature, at least from a practicality standpoint. However, an indirect account of this behavior was provided for in the model by assigning minimal axial stiffness to the elements used to model the vertical section of each facing unit. This prevented the modeled facing units from attracting any significant axial load, as was considered to be the case in the field-scale test.

Compaction

The observance of only 15 mm of vertical footing deflection under the maximum loading pressure of 356 kPa applied in the field-scale test confirms that compaction effects were significant, where the reinforced fill section of the field-scale test wall was constructed to 102 to 105 percent of the standard Proctor maximum dry density (appendix C). Implementation of the compaction effects in finite element modeling were discussed at length by Seed and Duncan.[(66)] They noted various theories and analytical procedures that could model one or more aspects of compaction, but also noted that none of these theories or procedures is reliable for predictive purposes. Various compaction modeling strategies were tested to assess their suitability using the observed load-deformation behavior as a basis of comparison. This lead to the adopted procedure where a 50 kPa inward pressure was applied to the top, bottom and exposed faces of

each lift to simulate compactive efforts, following activation of the lift which simulated initial placement. The inward pressure was then reduced to 10 kPa on the top and bottom faces prior to placement of the next lift to simulate vertical relaxation or unloading following compaction. The inward pressure acting on the exposed face was maintained at 50 kPa as this produced the most reasonable model deformation behavior compared with that observed in the field-scale test, and recognizing possible "locked-in" stresses.

While the adopted compaction procedure was considered the most realistic from a qualitative standpoint, modeled behavior still resulted in vertical footing displacements an order of magnitude greater than those observed. This aspect of the analysis was not resolved and the analyses reported in this appendix are considered to represent a lesser compacted sand than that used in the field-scale test. While this obviously affects interpretation from a quantitative standpoint, use of a lesser compacted sand was considered acceptable for interpreting failure characteristics in a qualitative sense.

D.2 ANALYSIS DETAILS

D.2.1 Soil

The mortar sand used to construct the reinforced fill in the Turner Fairbanks Highway Research Center (TFHRC) field-scale test was described as a poorly graded sand (SP) in terms of the Unified Soil Classification System (USCS). Particle size analysis reported the following: D_{10} = 0.15 mm, D_{30} = 0.24 mm, and D_{60} = 0.39 mm (C_u = 2.7, C_c = 1.05).[59] Laboratory direct shear test results for the sand produced a friction angle of 39 degrees at an equivalent dry density of 14.8 kN/m^3, corresponding to approximately 96 percent of the standard Proctor maximum dry density.[59] A cohesion of 4.0 kPa was inferred from results of borehole shear testing provided by TFHRC. Moisture-density testing conducted according to the method outlined in AASHTO T-99 provided a maximum dry density of 15.3 kN/m^3 at a moisture content of 17.4 percent, revealing that wall construction exceeded normal standards with greater than 100 percent compaction achieved.[7]

The sand was modeled using the advanced Hardening-Soil formulation available in PLAXIS, providing both shear and volumetric hardening capabilities based on hyperbolic stress-strain behavior. The Hardening-Soil model also features stress dependent stiffness according to a power law, elastic unloading/reloading behavior, shear failure according to the Mohr-Coulomb failure criterion, and tensile failure strength. Recourse to the work undertaken by Duncan et al. was made in order to provide a basis for establishing stress-strain parameters.[67] Duncan et al. back-fitted a hyperbolic stress-strain formulation to various sands tested in the triaxial device, providing particle size analysis data that was used as guidance in selecting appropriate parameters for the TFHRC mortar sand.[67] Comparison of resultant triaxial compression stress-strain curves for both models over small strain and large strain ranges at confining stress (σ_3) values of 101.3 kPa and 20 kPa are plotted in figures 83 and 84, respectively. These indicate sufficiently accurate agreement for modeling purposes. Soil parameters are provided in table 14 accordingly.

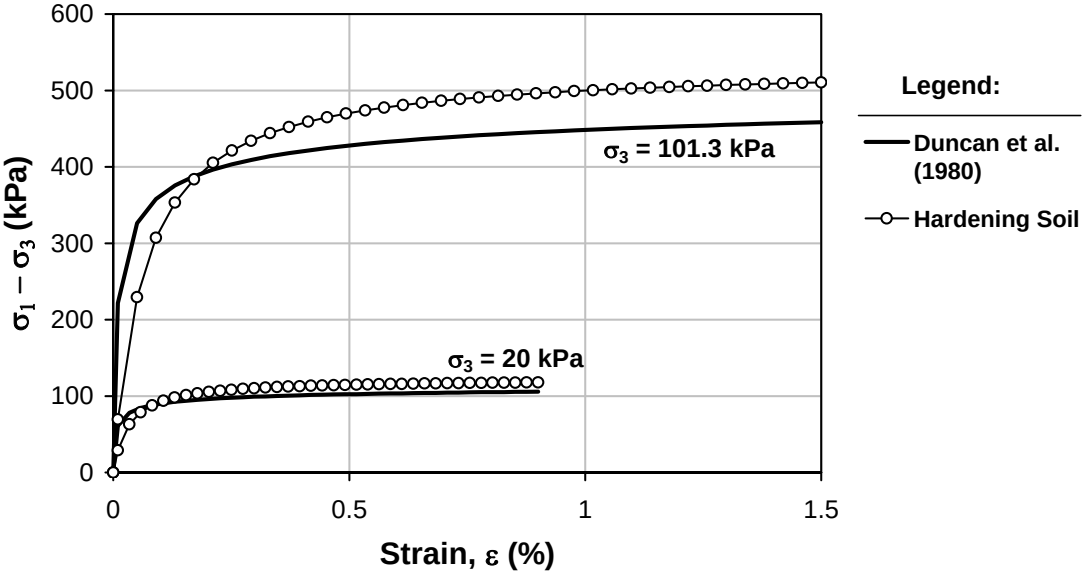

Figure 83. Graph. Stress-strain comparison over small strain range.

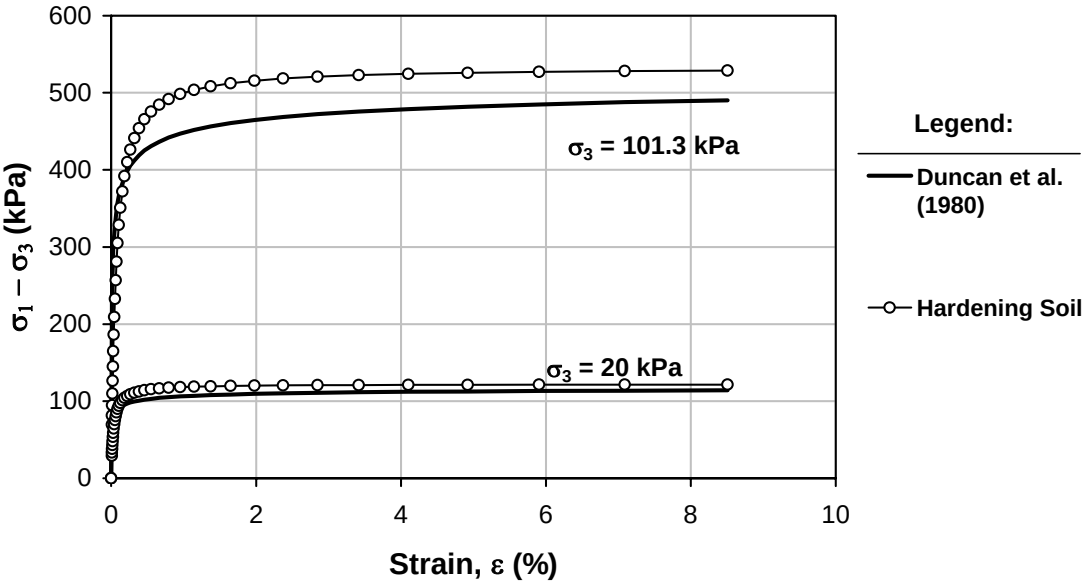

Figure 84. Graph. Stress-strain comparison over large strain range.

Table 14. Soil model parameters.

Parameter	Value
Unit weight (unsaturated), γ	14.8 kN/m^3
Effective cohesion, c'	4 kPa
Effective friction angle[1], ϕ'	44 degrees
Dilatancy angle, ψ_d	8 degrees
Power for stress-level dependency of stiffness, m	0.5
Reference secant modulus for deviatoric loading, E_{50}^{ref}	4000 kPa
Reference secant modulus for primary compression, E_{oed}^{ref}	4000 kPa
Reference secant modulus for unloading/reloading, E_{ur}^{ref}	8000 kPa
Poisson's ratio for unloading/reloading, ν_{ur}	0.2
Reference pressure for stiffness, p^{ref}	101.3 kPa
Tensile strength, $\sigma_{tension}$	0 kPa
Failure ratio, R_f	0.9

[1] Correction applied for plane strain conditions, based on Allen et al.(65)

D.2.2 Structures

Geometrical and Material Properties

Material and geometrical properties used for modeling the geogrid, MSE facing units, and the footing are provided in tables 15, 16, and 17, respectively.

Table 15. Modeling parameters for geogrid.

Parameter	Value
Axial stiffness per unit strain, *EA*	1,560 kN/m
Maximum tensile force, *F*	114 kN/m

Table 16. Modeling parameters for MSE facing units.

Component	Parameter	Value
Vertical Component	Axial stiffness per unit strain, *EA*	4 kN/m
	Bending stiffness, *EI*	0.12 kNm^2/m
	Moment capacity, M_p	2,000 kNm/m
	Axial force capacity, N_p	6 kN/m
	Poisson's Ratio, ν	0.3
	Unit weight, γ	0.046 kN/m/m
Diagonal Component	Axial stiffness per unit length, *EA*	10,900 kN
	Maximum compressive force, $F_{max,comp}$	17 kN
	Maximum tensile force, $F_{max,tens}$	17 kN
	Out of plane spacing, *L*	1.0 m

Table 17. Modeling parameters for loading footing.

Parameter	Value
Axial stiffness per unit strain, *EA*	1.32×10^7 kN/m
Bending stiffness, *EI*	2.74×10^5 kNm^2/m
Unit weight, γ	11.5 kN/m/m

Structure Models

Geogrids were modeled using "geogrid" elements possessing only one (axial) degree of freedom at each node, and an inability to sustain compressive forces. A maximum tensile force was also assigned to effect a limiting capacity state.

The vertical component of the MSE facing units were modeled using "plate" (beam) elements possessing x-translation, y-translation and a rotational degree of freedom at each node, and able to sustain axial forces. However, a low axial stiffness was assigned in order to minimize load carrying capabilities, as discussed in the "Modeling Issues" in section D.1.2. The diagonal (or strut) component of the wall facing was represented using an "anchor" element as previously discussed, representing what was essentially a spring element possessing a maximum axial force capacity (spring-slider element).

The reinforced concrete footing was modeled using a plate element assuming elastic behavior and using axial and flexural rigidities based on gross footing dimensions (i.e., ignoring the steel reinforcement). The various structure models are indicated on figure 85.

D.2.3 Model Configuration

The modeling configuration used for analysis purposes is shown in figure 85, indicating geometry, boundary, and loading conditions applied to the model. Model dimensions and wall facing batters corresponded to the field-scale test, i.e., vertical height equal to 5.5 m with a reinforcement base width of 1.4 m increasing to 2.2 m at the top. Lift thicknesses were modeled as 0.46 m, and additional geogrids were placed centrally in lifts 11 and 12 to approximate the constructed configuration. A fixed boundary at the location of the shoring wall face followed the assumption of a rigid boundary at this location. "Interface" elements were utilized at all structure-soil boundaries (not shown on figure 85 for clarity) to provide for possible slippage and separation, assuming strength equal to that of the soil (i.e., rough interface). Mesh discretization used in the analysis is shown in figure 86.

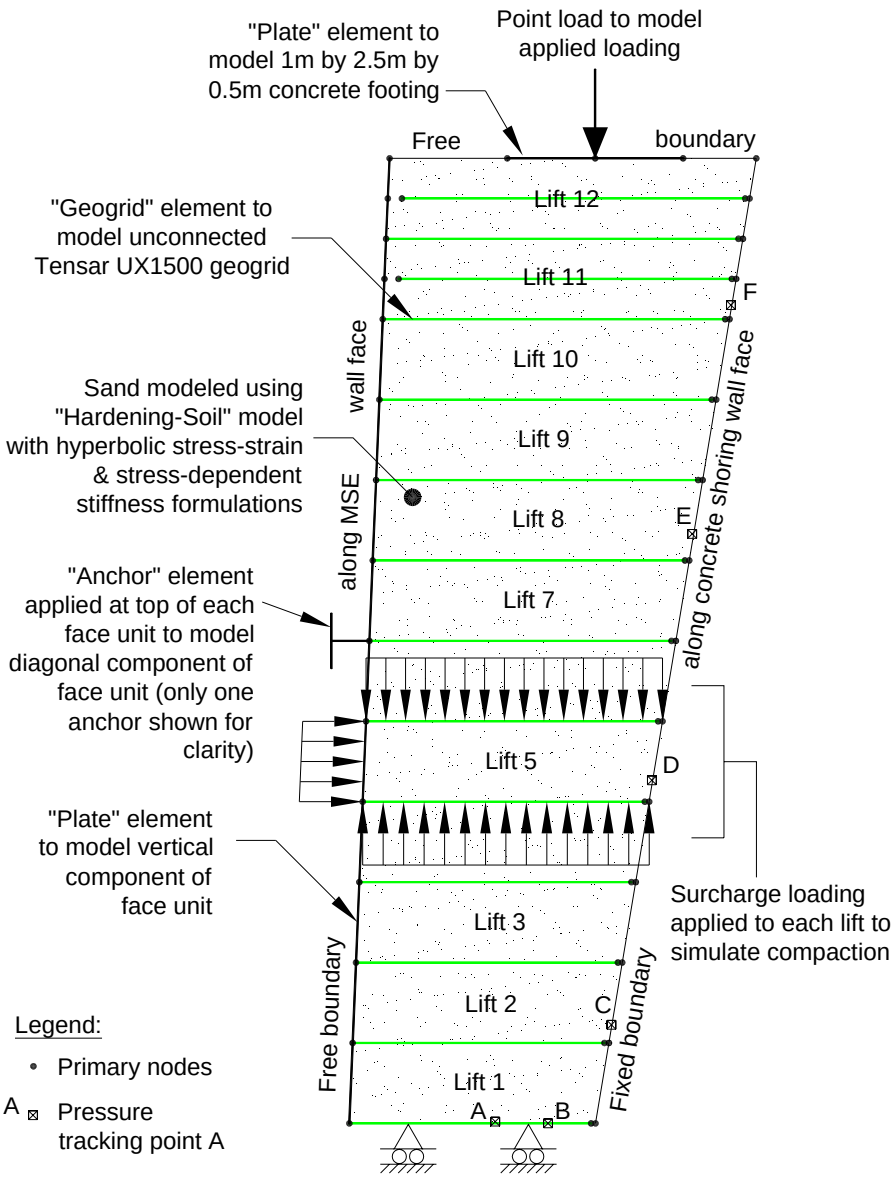

Figure 85. Diagram. PLAXIS field-scale test wall model configuration.

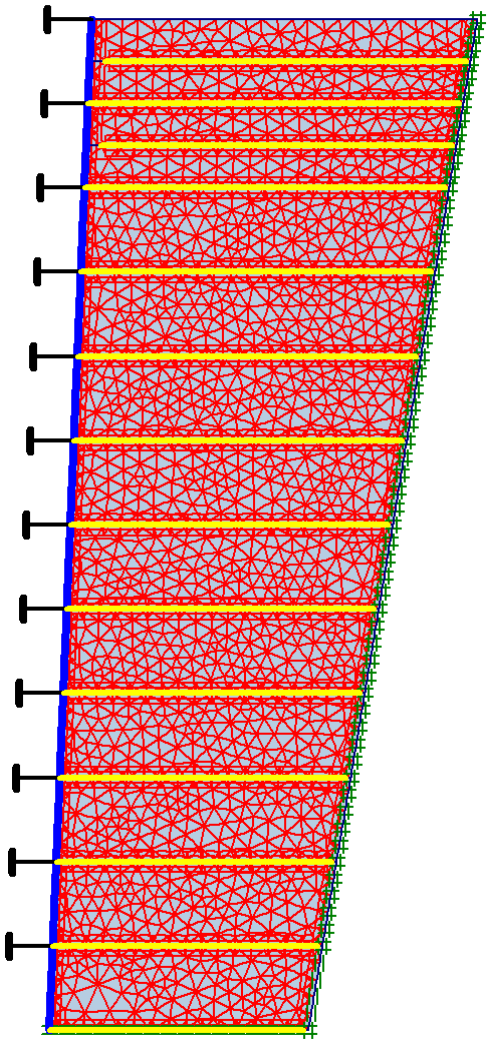

Figure 86. Screenshot. PLAXIS model mesh discretization.

D.2.4 Initial Stress State and Modeling Sequence

A pre-consolidation pressure of 50 kPa was applied to all lifts in recognition of compaction induced overconsolidation. The construction sequence adopted for modeling purposes proceeded as follows:

- Step 1 – Activate lift 1 and solve for self-weight loading.
- Step 2 – Apply 50 kPa compaction surcharge loading and solve.

- Step 3 – Reduce vertical surcharge loading to 10 kPa and solve.

- Repeat steps 1 through 3 for each lift.

Footing loading was simulated using a point load located at the center of the 1 m wide equivalent plate element (refer to figure 85). Loading was applied in 50 kPa increments.

D.3 ANALYSIS RESULTS

D.3.1 Geogrid Strain Behavior

Distribution of axial strain with footing load level in geogrid elements representing instrumented locations are shown in figures 87 and 88. The load range in figure 87 corresponded to the loading range applied in the field-scale test, whereas figure 88 provides additional data up to the load level approaching model failure (approximately 1,000 kPa). A general trend of increasing axial strain with increasing load level is apparent, as was observed in the field-scale test. The existence of some initial pre-stress in the geogrid elements at the MSE face is noted, attributed to the unloading procedure applied to model compaction effects. Such behavior was not observed in the field-scale test, but given the proximity to the free face and effective removal of pre-stress with increasing load levels, the effect of this pre-stress force was considered to have had only minimal influence on model failure characteristics.

Similarities between the modeled and field-scale geogrid behavior are otherwise apparent: (1) both exhibited decreasing strain levels with decreasing wall height at a given footing pressure, and (2) both exhibited varying strain levels along each geogrid layer, with a distinct increase in strain noted towards the center of the footing in the upper geogrid layers.

D.3.2 MSE/Shoring Interface Pressure Behavior

Plots of lateral and vertical pressure behavior at points representing locations of the pressure load cells used in the field-scale test are shown in figures 89 and 90, respectively. The lateral and vertical pressure data correspond to the loading range applied in the field-scale test, using the same plotting format as used to present the field-scale test data (appendix C). Comparison with the field-scale test data indicates similar trends of increasing lateral and vertical pressures with increasing loads, but marked differences in the distribution of lateral and vertical pressures with wall height. Namely, the model results indicate lateral and vertical pressures generally increase toward the top of the wall, whereas the field-scale data indicate lateral and vertical pressures generally decrease with wall height. These differences are attributed to the modeled construction process, in particular the compaction procedure adopted for modeling purposes, and highlights the difficulty in modeling an appropriate initial stress state with the MSE shoring wall system, as alluded to in the discussion of modeling issues.

In order to help assess pressure behavior in a qualitative sense, plots of stress-strain behavior recorded at the tracking points are shown in figures 91 and 92, indicating lateral and vertical pressure behavior, respectively, for the entire loading range applied in the model. The location of the tracking points, labeled A through F in figures 91 and 92, are indicated on figure 85.

Pressure at the shoring face at the level of lift 2 is characterized by a marked reduction in pressure compared to the remaining locations. This effect is also apparent at the lift 5 level, although to a much lesser degree, and a distinct drop in vertical pressure near model failure is also apparent at the base location nearest the shoring face.

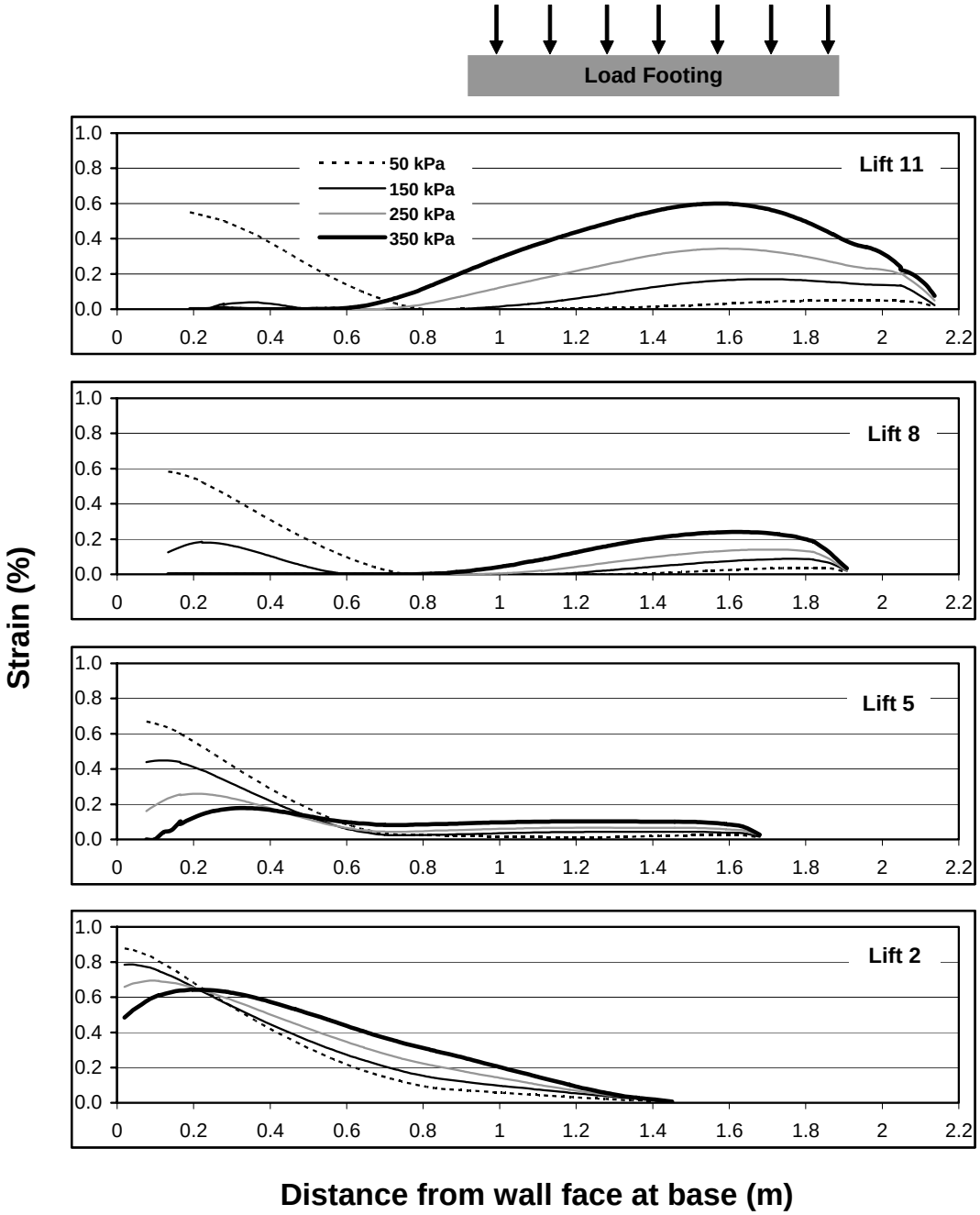

Figure 87. Graph. Calculated strains in geogrid layers over field-scale test load range.

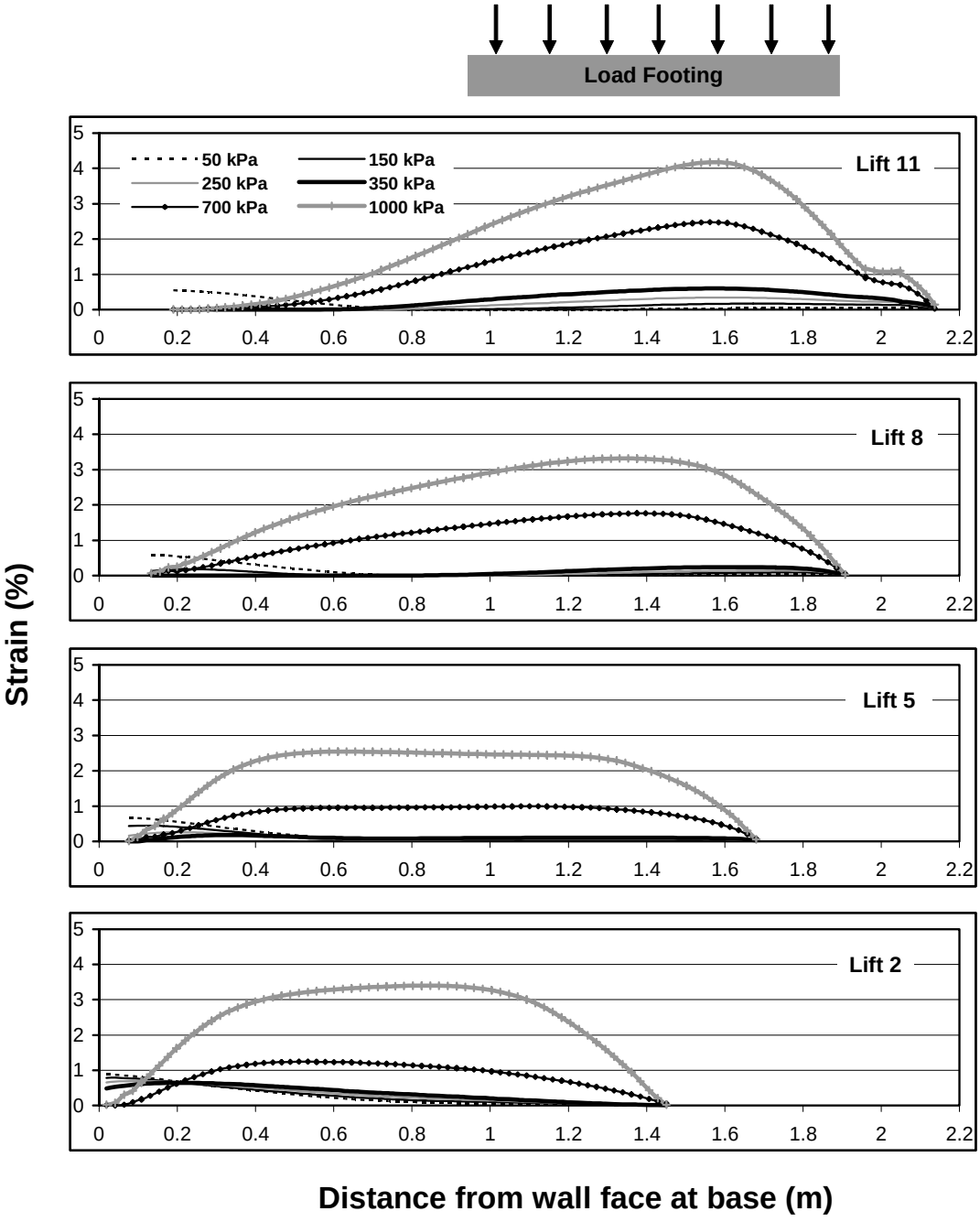

Figure 88. Graph. Calculated strains in geogrid layers over model load range.

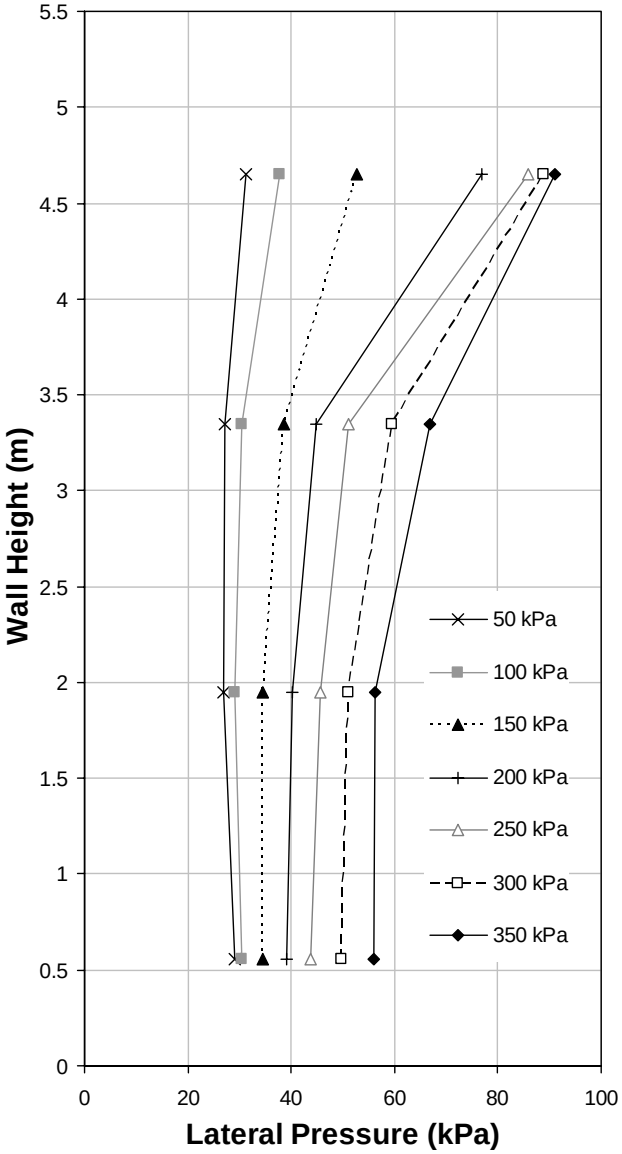

Figure 89. Graph. Lateral pressures recorded at tracking points for footing pressures up to 350 kPa.

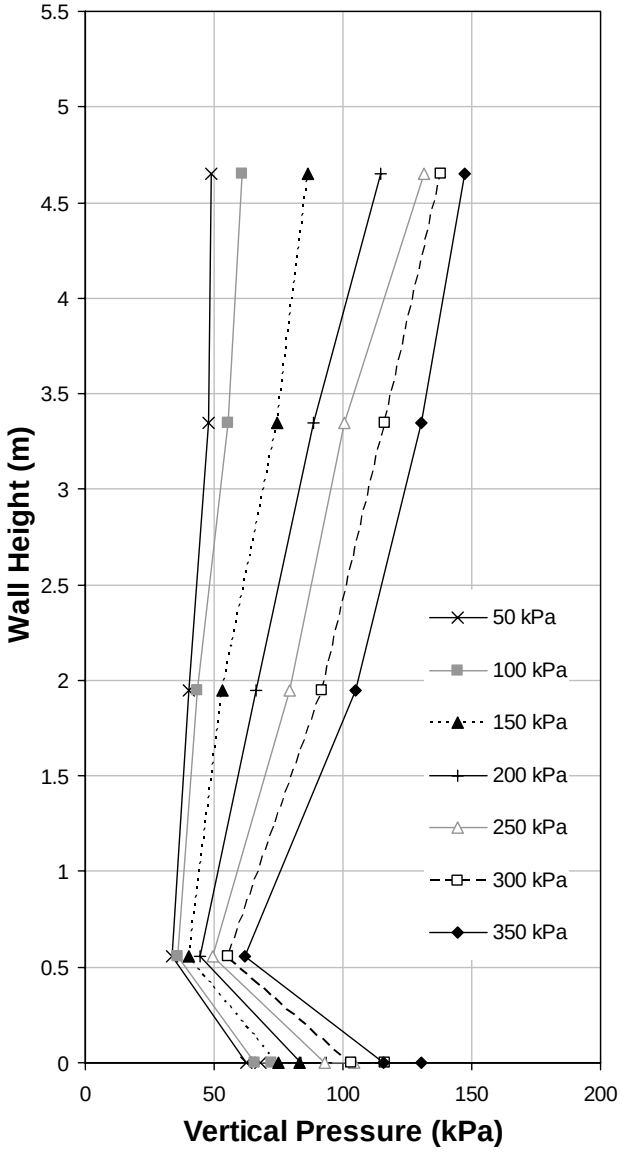

Figure 90. Graph. Vertical pressures recorded at tracking points for footing pressures up to 350 kPa.

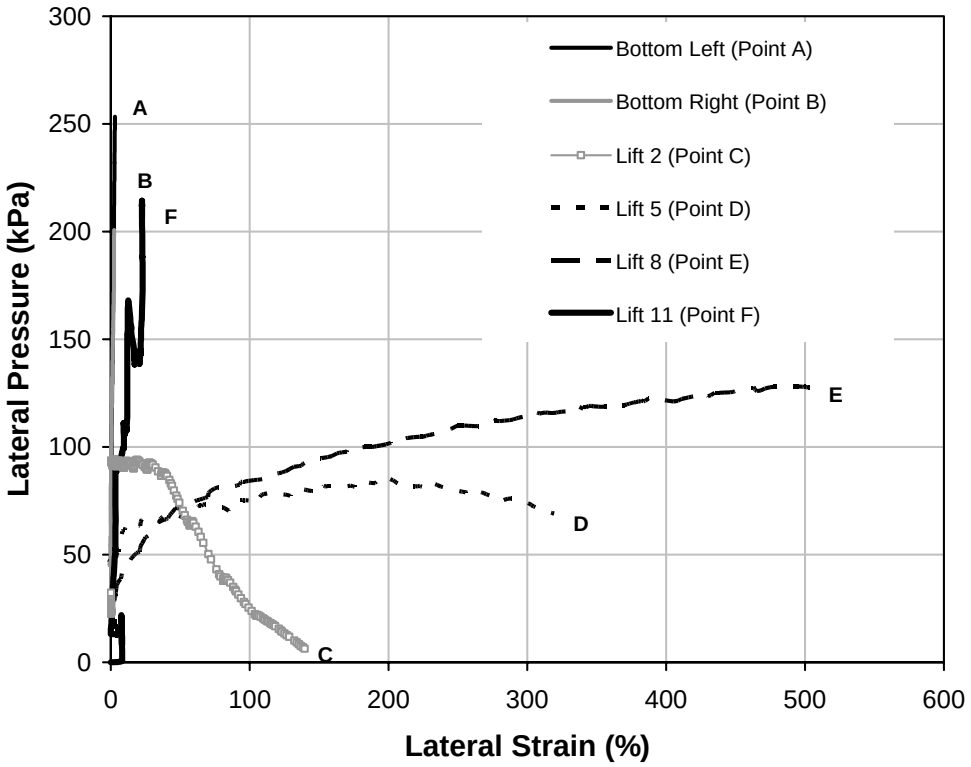

Figure 91. Graph. Lateral pressures recorded at pressure tracking points.

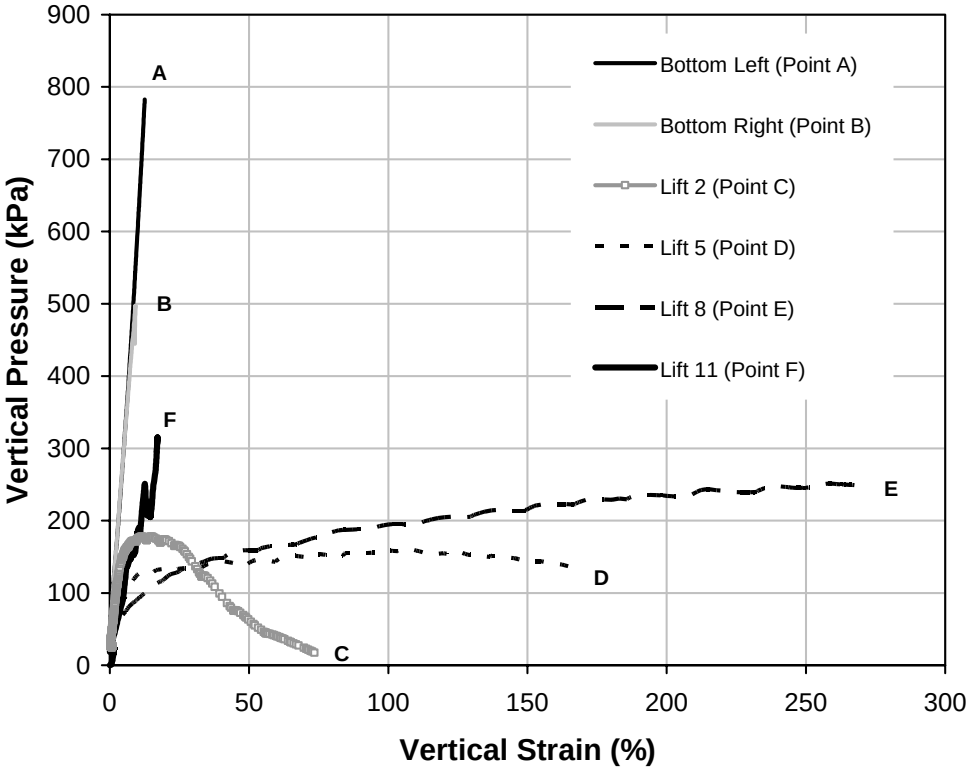

Figure 92. Graph. Vertical pressures recorded at pressure tracking points.

D.3.3 Failure Characteristics

Principal stress direction and shear failure stress behavior are considered most representative of the failure characteristics exhibited by the model. Plots of principal stress directions at footing loads of 50 kPa and 1,050 kPa (just prior to model failure) are shown in figures 93 and 94, respectively. Corresponding contour plots of relative shear, defined as the ratio of induced shear stress to failure shear stress, are shown in figures 95 and 96, respectively. These plots summarize a progressive increase in shear stress at the shoring face, increasing with depth and with increasing load level, leading to failure (slippage) with subsequent load shedding to lower levels. This load shedding evolves into a more vertical load path of resistance with increasing load level, and results in an arching effect at the bottom inside corner area with associated reduction in pressure.

Ultimate failure of the model is brought about by diminishment of a "core" of unfailed material serving to transmit the applied load to the model base. This core reaches a critical configuration near the base of the model where Rankine-type shear failure zones pervade it, leading to collapse.

D.4 CONCLUSIONS

Qualitative agreement between field-scale test and model observations was achieved indicating validity of the numerical approach undertaken. Model results suggest a failure load corresponding to approximately three times the load applied in the field-scale test (i.e., 1,100 kPa vs. 350 kPa). While the findings clearly indicate the required reinforcing effect of the geogrids, the model failure characteristics suggest that ultimate failure may be essentially a soil failure mechanism brought about by the narrow width of the MSE wall at its base, further supporting use of a minimum reinforcement width of 0.3*H*.

In addition, the plot of shear contours prior to failure (figure 96) supports the centrifuge modeling (appendix B) and field-scale testing (appendix C) results with regard to the following:

- Contours at the top of the wall beneath the load footing are indicative of bearing capacity failure, as was observed from the phase II centrifuge modeling.

- Tension is observed at the shoring interface which was supported by the tendency for the model walls to "pull away" from the shoring wall during the centrifuge modeling, and may have resulted in poor performance of the vertical earth pressure cells installed in the field-scale test.

The observed tension at the shoring interface further supports the recommendation to extend upper MSE reinforcements over the shoring interface.

The modeling efforts undertaken also demonstrate the sensitivity of model behavior to various issues, and indicate the need for attention to detail and to question the model results. While the qualitative behavior of the model was considered reasonable, it is clear that compaction effects warrant further investigation to achieve quantitative agreement with field-scale results.

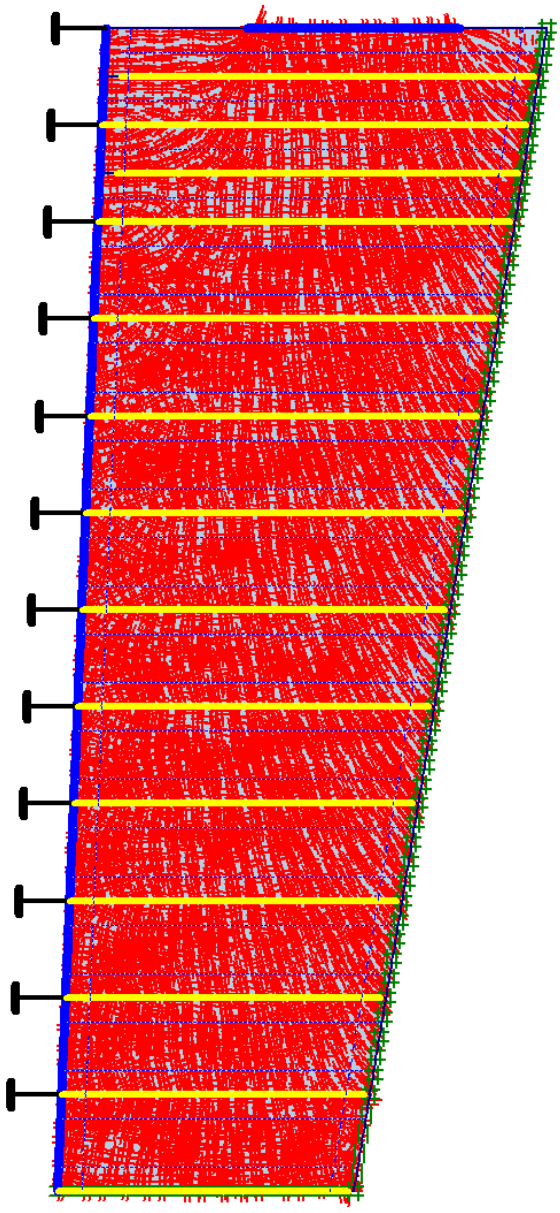

Figure 93. Screenshot. Principal stress directions at footing loading of 50 kPa.

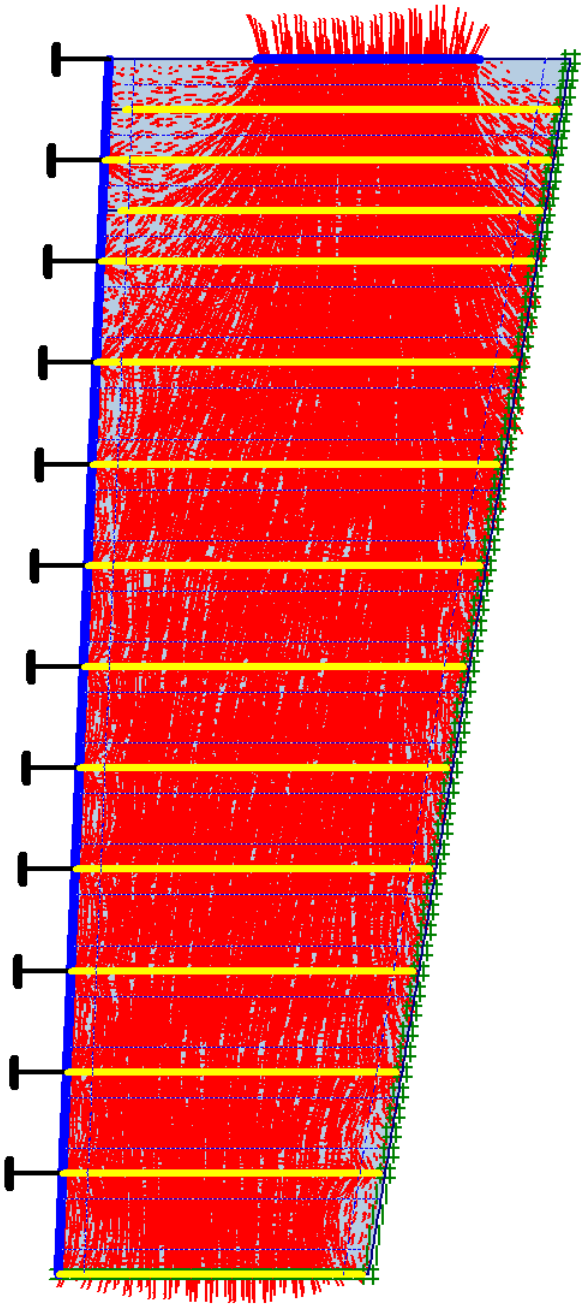

Figure 94. Screenshot. Principal stress directions prior to failure (footing loading = 1,050 kPa).

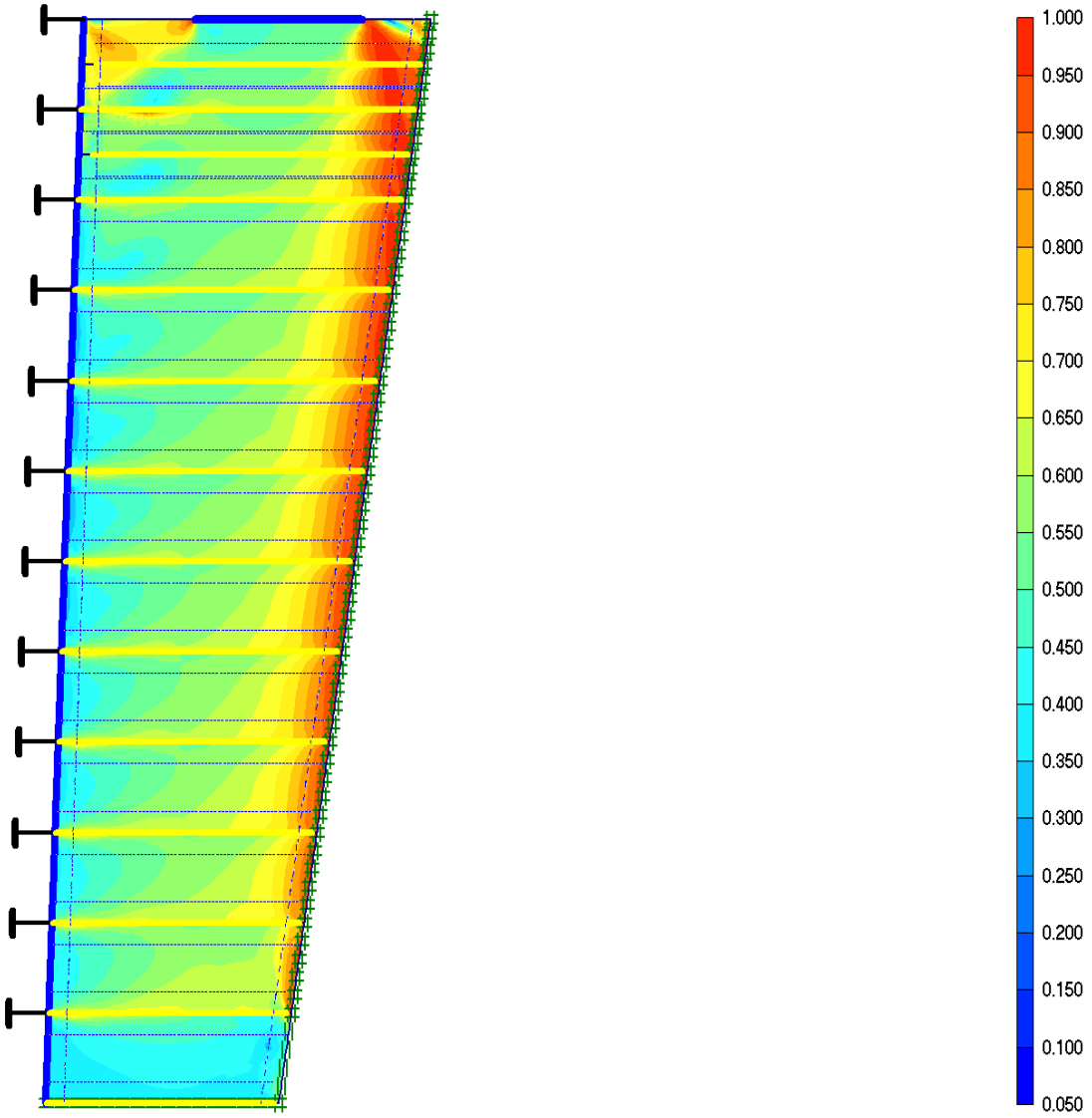

Figure 95. Screenshot. Relative shear contours at footing loading of 50 kPa.

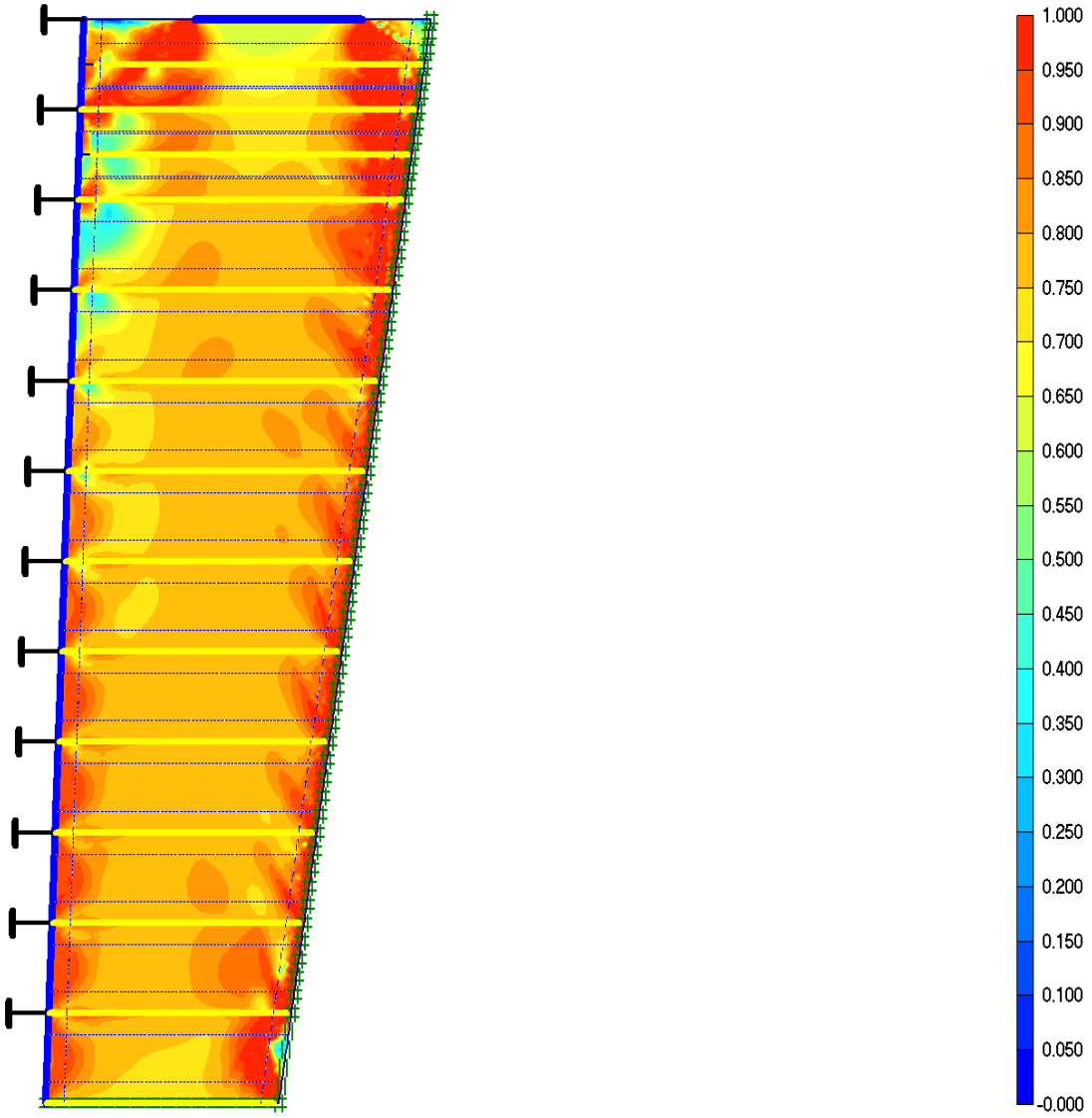

Figure 96. Screenshot. Relative shear contours prior to failure (footing loading = 1,050 kPa).